Integrated experimental and kinetic analysis of methane pyrolysis: Mapping the effects of temperature and residence time for hydrogen production

Sooyong Lee[a], Young Duk Lee[a]*

[a] Department of Energy Engineering, Korea Institute of Energy Technology (KENTECH), 21 KENTECH-gil, Naju, Jeollanamdo 58330, South Korea, leesoo9352@kentech.ac.kr
** Corresponding Author: ydlee@kentech.ac.kr*

Abstract:

Methane pyrolysis, which thermally cracks methane into hydrogen and solid carbon without carbon dioxide emission. The process can be economically feasible selling carbon for various industrial applications, such as tire, rubber, plastic. It means this process can reduce hydrogen production costs. By those economic and environmental benefits, methane pyrolysis is an alternative pathway for clean hydrogen energy. But the methane pyrolysis plant is still in small-scale. Despite these environmental and economic benefits, scaling up methane pyrolysis plants remains a challenge due to carbon deposition and a lack of robust kinetic models for reactor design.

This study investigated methane pyrolysis through an integrated approach with process simulation, experimental, and reaction kinetic modeling approaches. First, a plasma-assisted methane pyrolysis process was conceptualized to highlight the necessity of accurate kinetic models under nitrogen dilution. Subsequently, the experiment was conducted using a fixed-bed ceramic reactor at temperatures over 1200°C. The maximum methane conversion was calculated to be 97% at 1400°C. Furthermore, expanding the reactor inner diameter from 23 mm to 50 mm effectively mitigated carbon clogging, extending the continuous operation time to over 12 hours. Based on experimental data, kinetic parameters were optimized for both a single-step global reaction and a two-step series reaction mechanism. For the single-step reaction, two distinct plug flow reactor (PFR) mathematical models were compared to accurately account for gas-phase volume expansion, yielding activation energies of 155.46 and 141.01 kJ/mol, respectively. Finally, 3D parametric mapping was utilized to visualize the interconnected effects of temperature, residence time, and initial methane concentration on conversion, providing a comprehensive guideline for the design and optimization of scalable methane pyrolysis reactors.

Keywords:

Hydrogen; Methane Pyrolysis; Methane conversion; Residence time; Kinetic parameter.

1. Introduction

The global demand for hydrogen has steadily increased due to its utilization as an energy carrier across various industrial sectors, including power generation, transportation, and chemical synthesis. And the International Energy Agency (IEA) announced that to meet net zero emissions by 2050, 530 Mt of hydrogen is needed. To meet the demand of hydrogen, various hydrogen production methods are indicated shown in Table 1. Table 1 summarized various processes using fossil fuels and electricity, listing each process its representative chemical reaction. The dominant method is utilizing natural gas for producing hydrogen due to its low cost. And most of the hydrogen 96% is produced from fossil fuels, especially natural gas [1]. The most commercial hydrogen production method is steam reforming, which is cost-effective, utilizing natural gas and steam. However, this method emits lots of carbon dioxide emissions. To reduce emissions, carbon capture and storage (CCS) technologies and syngas production have emerged. Although producing syngas by reacting natural gas with steam, carbon dioxide or oxygen, they cannot avoid generating CO_2 as a byproduct in intermediate steps, meaning they are not entirely clean or carbon-free methods.

Table 1. *Various Hydrogen production methods.*

Process	*Energy source*	*Reaction*
Coal gasification	Coal	$C(char) + O_2 \rightarrow CO_2$
Steam reforming	Natural gas	$CH_4 + H_2O \rightarrow CO + 3H_2$ $CO + H_2O \rightarrow CO_2 + H_2$
Partial oxidation	Natural gas	$CH_4 + 1/2O_2 \rightarrow CO + 2H_2$
Dry reforming	Natural gas	$CH_4 + CO_2 \rightarrow 2CO + 2H_2$
Auto-thermal reforming	Natural gas	$CH_4 + H_2O \rightarrow CO + 3H_2$ $CH_4 + 1/2O_2 \rightarrow CO + 2H_2$
Bi-reforming	Natural gas	$CH_4 + H_2O \rightarrow CO + 3H_2$ $CH_4 + CO_2 \rightarrow 2CO + 2H_2$
Pyrolysis	Natural gas	$CH_4 \rightarrow C + 2H_2$
Water electrolysis	Electricity	$H_2O \rightarrow H_2 + 1/2O_2$

Various methods with natural gas as energy source have associated CO_2 emissions and are thus not carbon neutral. However, methane pyrolysis is an endothermic reaction, which converts methane into hydrogen and solid carbon that does not emit any emissions. It has economic advantageous of selling carbon which can reduce the hydrogen production cost. In chemical equilibrium conditions, Figure 1(a) shows the reaction results of methane pyrolysis at different temperatures and Figure 1(b) illustrates the gas composition among the products except for hydrogen. Methane pyrolysis in overall reaction can be expressed as stepwise dehydrogenation at high temperatures: $2CH_4 \rightarrow C_2H_6 \rightarrow C_2H_4 \rightarrow C_2H_2 \rightarrow 2C$ [2]. The calculation result shows that methane can be decomposed into various products, not just hydrogen and carbon. And in real conditions, methane pyrolysis starts at above 1000°C without a catalyst and more gaseous hydrocarbon product could produce.

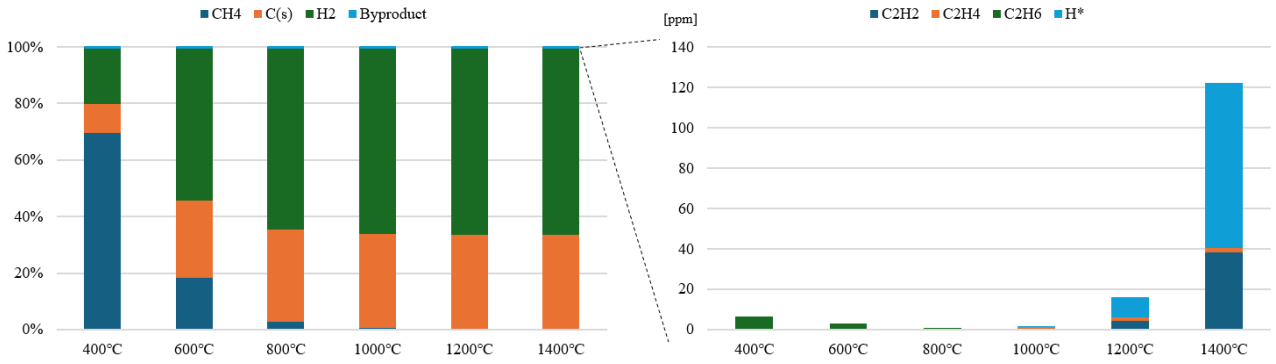

(a) (b)

Figure. 1(a): *Gas fraction of methane pyrolysis at equilibrium conditions* ***(b):*** *Main byproducts of methane pyrolysis at each temperature.*

While extensive research is being conducted on various catalysts to reduce reaction temperatures, carbon deposition leads to catalyst deactivation, making them unsuitable for long-term operation. As a potential solution, molten salt and molten metal catalysts have been introduced [3]. Their liquid phase helps prevent carbon deposition due to density difference. However, their high energy demands sustaining catalyst liquid phase make them impractical for large-scale up.

In this background, research on methane pyrolysis has been actively ongoing. Various methane pyrolysis fundamental research has been carried out, including experimental study, kinetic modeling and reaction mechanism.

Lott et al. constructed the non-catalytic methane pyrolysis experiment and focused on byproduct gas. They found that gaseous byproducts concentrations calculated about total volumetric approximately 1.7%. Increasing the input of H_2, CH_4 ratio resulted in a reduction of methane conversion. Also, it demonstrated advantageous with preventing the byproduct formation and solid carbon deposition [4].

Dahl et al. conducted a kinetic study using an aerosol flow reactor, performing experiments at temperatures ranging from 1533-2144 K and residence time between 0.9 and 1.5 s [5]. Trommer et al. investigated a carbon-seeded reactor experimentally at temperatures above 900 K, with residence time of 9 s and an initial methane concentration between 0.09 and 0.15 [6]. Rodat et al. carried out a kinetic analysis based on experimental results from a tubular solar reactor, using initial methane mole fraction ranging from 0.1 to 0.33, reported kinetic parameters of pre-exponential factor 6.6·1013 s^{-1} and an activation energy of 370 kJ/mol [7].

Celik et al. examined the methane pyrolysis mechanism with modified combustion of light hydrocarbon kinetic mechanism [8]. Koshi et al. examined detailed chemical mechanisms to simulate hydrogen and pyrocarbon production during methane pyrolysis and results suggested the deposited carbon is disordered and catalytic, not graphene-like [9]. The application of detailed chemical mechanisms in CFD analysis remains challenging due to the excessive computational cost. Consequently, Vargas et al. utilized a detailed chemical mechanism, applying a genetic algorithm to reduce the number of reactions and species to 10 each [10]. While numerous detailed mechanisms and reduced mechanisms for methane pyrolysis have been proposed by excluding oxidation pathways from combustion models, their implementation in computational fluid dynamics remains challenging due to the high computational costs associated with hundreds of chemical species and complex reactions.

To bridge the gap between process scale-up and fundamental kinetics, this study employs an integrated approach. First, a process simulation for plasma-assisted methane pyrolysis is presented to demonstrate the critical need for a robust kinetic model that accounts for the nitrogen dilution effect. Experimentally, the effects of temperature and volumetric flow rate on methane conversion were evaluated. The influence of reactor size on operation stability was also studied by varying the reactor diameter, demonstrating that increasing the inner diameter significantly extend continuous operation time. To develop the chemical kinetic model, two distinct reaction mechanisms were evaluated: a single-step global reaction ($CH_4 \rightarrow C + 2H_2$) and a two-step series reaction ($2CH_4 \rightarrow C_2H_2 + 3H_2$ & $C_2H_2 \rightarrow 2C + H_2$). For the single-step pathway, two different PFR mathematical models were selected to optimize the kinetic parameter. After tuning and validating the kinetic parameters against experimental data, the models were employed to estimate methane conversion and reactor performance.

2. Process simulation: Plasma-assisted methane pyrolysis

As illustrated in Figure 2, the process integrates a plasma-assisted reactor with downstream separation and recycling unit; detailed parameters and specifications are summarized in Table 2. The process initiates by co-feeding natural gas and nitrogen gas into plasma reactor at an equimolar ratio (1:1). Following pyrolysis, the product gas is quenched to 200 °C using a heat exchange and cooling unit to halt secondary reactions, minimizing the formation of polycyclic aromatic hydrocarbons (PAHs). Subsequently, solid carbon particles are removed via a cyclone and fabric filter assembly. Finally, the unreacted gas and hydrogen are separated from the product stream and residual gas recycled back to the reactor inlet to maximize feedstock utilization.

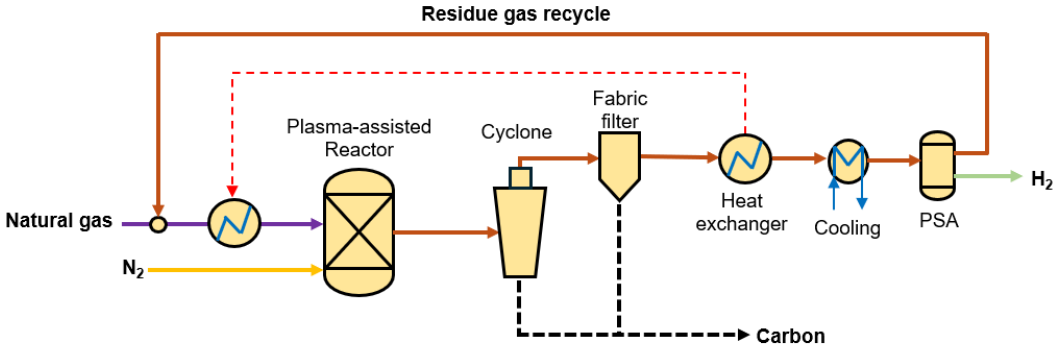

Figure. 2. *Process flow diagram of plasma-assisted methane pyrolysis plant*

Table 2. *Natural gas composition*

Composition	CH_4	C_2H_6	C_3H_8	i-C_4H_{10}	n-C_4H_{10}	i-C_5H_{12}	n-C_5H_{12}	N_2
%	92.719	5.207	1.301	0.281	0.304	0.014	0.009	0.166

A critical operational feature of this system is the continuous co-feeding of nitrogen. Subjecting pure natural gas to a plasma torch induces instantaneous carbon deposition near the electrodes, which leads to coking and reactor clogging. The introduction of nitrogen mitigates this issue; acting as an inert diluent, it stabilizes the plasma discharge and protects the internal reactor components. However, this volume of nitrogen complicates the reaction hydrodynamics. The inert gas elevates the total volumetric flow rate, reducing the actual residence time of the reactants within the high-temperature zone. When coupled with the inherent volumetric expansion characteristic of methane pyrolysis, this dilution creates a non-linear reacting flow.

Initially, the reactor performance in the process simulation was calculated under chemical equilibrium conditions. In the actual process, however, other hydrocarbon intermediates are detected, and the practical methane conversion and hydrogen yield differ from these equilibrium predictions. Since the specific operating conditions of the downstream PSA unit depend directly on this product distribution, relying solely on equilibrium data is insufficient. Consequently, predicting the exact methane conversion and sizing the separation units for process scale-up necessitates a kinetic model that accounts for both volumetric expansion and nitrogen dilution effects.

3. Experimental study

Figure 3 illustrates the flow diagram of the methane pyrolysis experimental system. A ceramic alumina tube was selected for the reactor to withstand the maximum operating temperature of 1400 °C. The furnace temperature was precisely monitored using an R-type thermocouple. To reach the target reaction temperature, the electric furnace was heated over a period of 4.5 hours under continuous N_2 purging. Once the target temperature was stabilized, CH_4 was introduced into the reactor.

All gas flow rates were regulated by mass flow controllers (MFC, Brooks Instruments). It should be noted that oxygen, air, and water were utilized exclusively for reactor decoking (carbon removal) and were not present during the pyrolysis reaction. At the reactor outlet, a water-cooling was positioned to maintain structural stability and ensure the effluent gas reached room temperature. The downstream gas passed through a capture vessel for carbon collection before the remaining gas was exhausted.

The composition of the product gas was analyzed using gas chromatography (GC, Agilent 8890C) at 10-minute intervals. The GC system was equipped with both Thermal Conductivity Detectors (TCD) and Flame Ionization Detectors (FID) to ensure comprehensive detection of the product species. Quantitative analysis was performed using a calibration method based on high-purity reference gases (N_2, H_2, CH_4, C_2H_2). To protect the GC columns from carbon contamination, an in-line filter was incorporated into the sampling line. Detailed experimental conditions are summarized in Table 3.

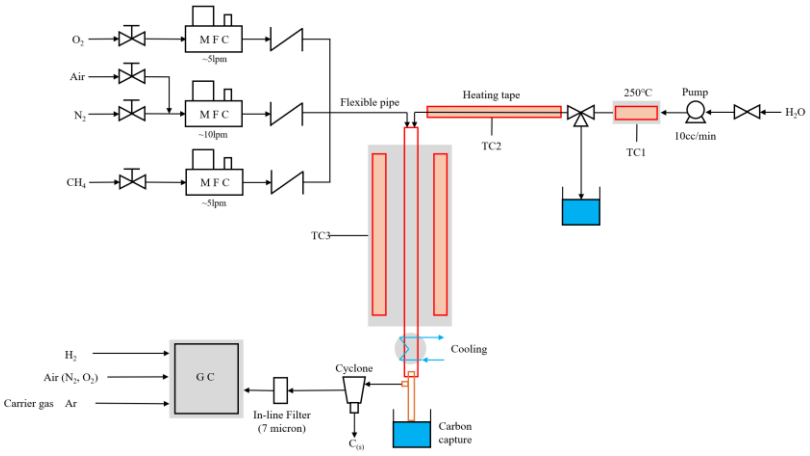

Figure. 3. *Flow diagram of methane pyrolysis experiment setup*

Table 3. *Experimental conditions*

Parameter	Specification
Reactor	Alumina tube (Al_2O_3)
Inner diameter (ID)	13, 23, 50 mm
Outer diameter (OD)	20, 30, 60 mm
Reactor length	650mm
Pressure	1 bar
Temperature	1200-1400 °C
CH_4 flow rate	1-3 Lpm
Residence time	0.5-1.5 sec

To evaluate the methane pyrolysis reaction, methane conversion and hydrogen yield are the key parameter. The methane conversion represents the concentration of methane consumed during the process, as defined in (1).

$$X_{CH4} = \frac{Q_{CH4,in} - Q_{CH4,out}}{Q_{CH4,in}}, \quad (1)$$

Where, $Q_{CH4,in}$ and $Q_{CH4,out}$ are volumetric flow rate of methane at the reactor inlet and outlet. The inlet measurement controlled by MFC, while the outlet flow rate was determined by GC measurement, calculated from the product gas composition.

The variation in CH_4 conversion with reaction temperature 1200-1400 °C and CH_4 flow rate (1-3 Lpm) with ID of 13 mm is presented in Figure 4. The pyrolysis was significantly enhanced by increasing temperature, demonstrating the dominant role of thermal energy in overcoming the reaction's kinetic barriers. At 1400 °C, the CH_4 conversion converged to a value above 97%, indicating that the influence of residence time becomes negligible at sufficiently high temperatures. Conversely, at 1200 °C, the residence time controlled by the flow rate, showed a more impact on CH_4 conversion, 1 Lpm case was 16.67% higher than that of the 3 Lpm case. This highlights that while residence time affects the CH_4 conversion at lower temperatures, the reaction is primarily governed by temperature in the high-temperature regimes.

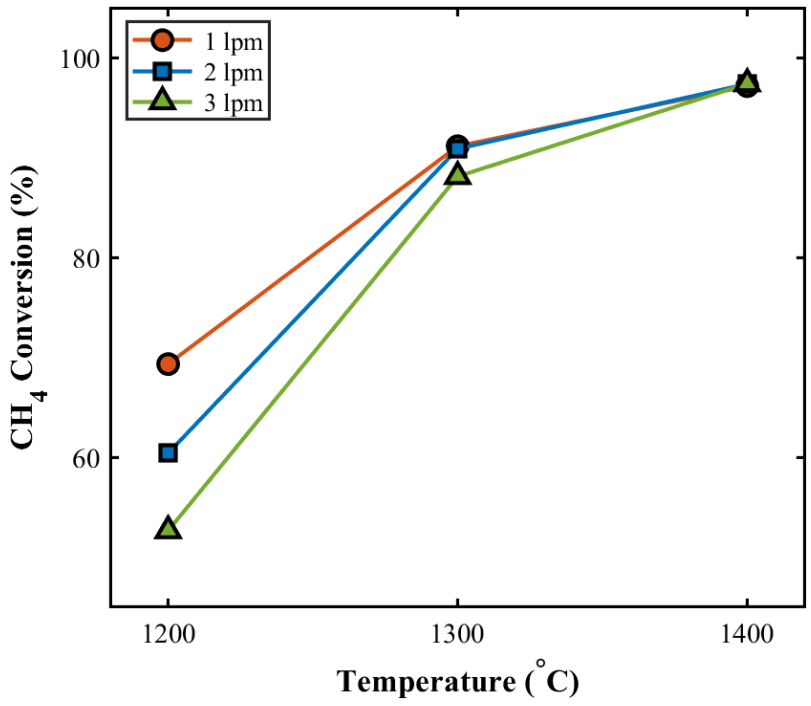

Figure. 4. *CH_4 conversion as function of feed flow rate and reaction temperature (CH_4 flow rate of 1-3 Lpm, fixed N_2 flow rate of 0.1 Lpm)*

The hydrogen yield (Y_{H2}) is defined as (2), the ratio of the inlet methane flow rate ($Q_{CH4,in}$) to the reacted methane ($Q_{CH4,reaction}$). $Q_{CH4,reaction}$ denotes the flow rate of methane converted into hydrogen through the reaction, while $Q_{H2,out}$ contents the flow rate of hydrogen at the reactor outlet.

$$Y_{H2} = \frac{Q_{CH4,reaction}}{Q_{CH4,in}} = \frac{1}{2}\frac{Q_{H2,out}}{Q_{CH4,in}}, \qquad (2)$$

Figure 5 illustrates the influence of initial CH_4 concentration and reaction temperature on CH_4 conversion (solid lines) and H_2 yield (dash lines). The experiments were performed using ceramic reactor with ID of 23 mm. a key observation is the significant enhancement in H_2 yield as the initial CH_4 concentration decreased from 1/2 to 1/4. This inverse relationship between feed concentration and Y_{H2} was consistently observed across the range of 1300-1400°C. At 1400°C, the Y_{H2} reached its peak of 75% when the CH_4 was diluted to a 1/4 ratio.

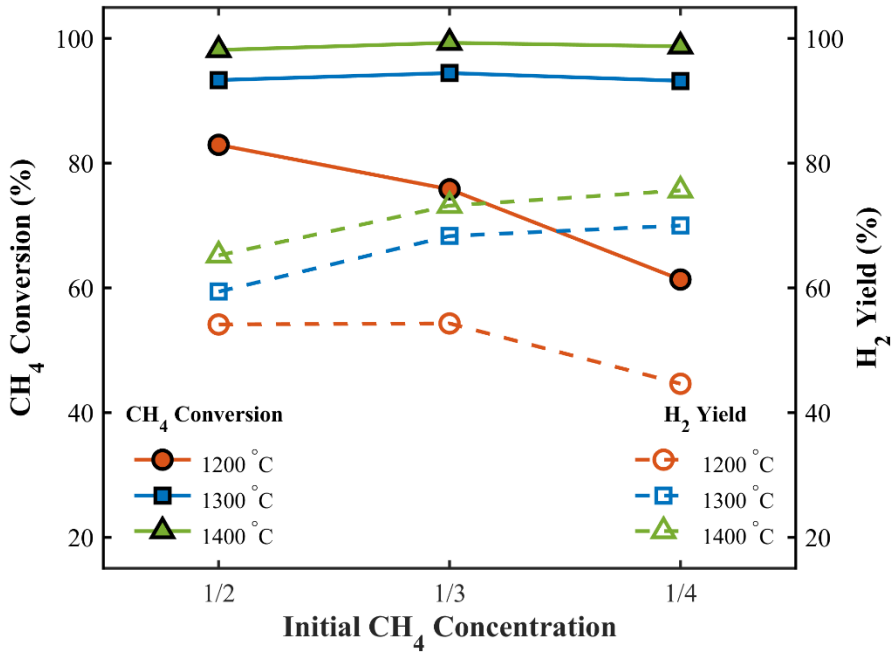

Figure. 5. *CH_4 conversion and H_2 yield as function of initial CH_4 concentration in an ID 23 mm*

To further elucidate the chemical pathways governing these yield trends, Figure 6 presents the measured experimental gas composition. The analyzed species included H_2 (blue), unreacted CH_4 (orange), and the intermediate hydrocarbon C_2H_2 (green). At higher temperatures of 1300 °C (b) and 1400 °C (c), the experimental results show the composition remains relatively stable regardless of the initial feed ratio, suggesting that the temperature is sufficient to rapidly drive the decomposition of both methane and its intermediate species.

In contrast, the data at 1200 °C (a) exhibits distinctly different experimental trend. A significant amount of unreacted CH_4 remains and 0.75-1.35% of C_2H_2 is observed in product stream. This accumulation of C_2H_2 indicates that while the primary decomposition of methane is active, the subsequent step, the decomposition of acetylene into hydrogen and solid carbon, is kinetically limited at this lower temperature. The clear dependency of the H_2 and C_2H_2 fractions on the initial methane concentration further suggests that the reaction is highly sensitive to the partial pressure of the reactants in this specific temperature range.

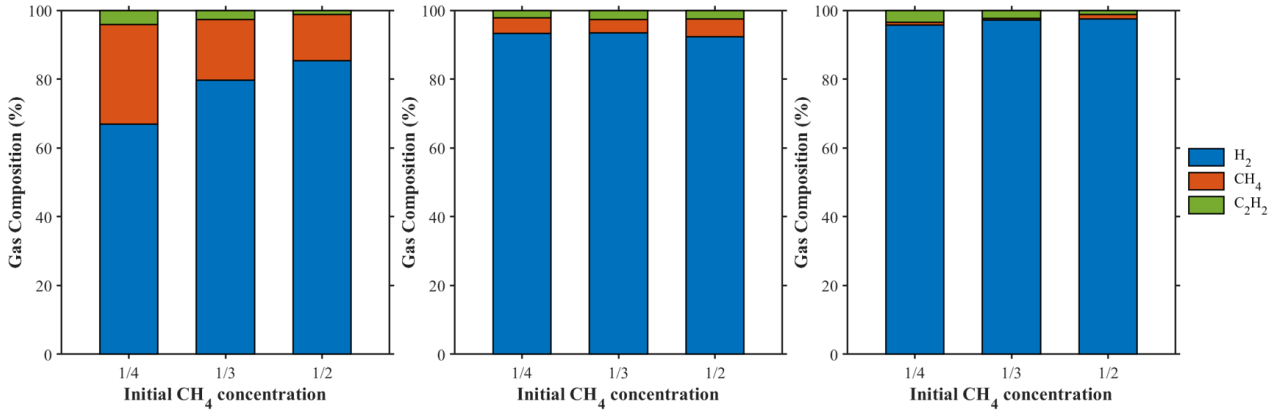

Figure. 6. *Observed experimental product gas composition at different reaction temperatures: (a) 1200 °C, (b) 1300 °C, (c) 1400 °C (Measured via GC)*

4. Kinetic modeling methodology

In chemical engineering, choosing appropriate reactor types is essential for facilitating chemical reactions and estimating the extent of reactant conversion into desired products. Among various reactor configurations, plug flow reactors (PFR) are widely employed for reaction kinetics modeling due to their well-defined characteristics, which allow for precise control of residence time and concentration variables along the reactor length. Unlike continuous stirred-tank reactors (CSTRs), PFRs exhibit minimal back-mixing and maintain a unidirectional flow, closely approximating ideal conditions. This makes them particularly suitable for capturing the intrinsic kinetics of gas-phase reactions under steady-state conditions, thereby providing reliable and scalable data for simulation and reactor design.

Based on a review of literature, two PFR models were adopted to optimize the kinetic parameters. In this study, models utilized kinetic fitting for two distinct reaction pathways: a single-step global reaction ($CH_4 \rightarrow C + 2H_2$) and a two-step series reaction ($2CH_4 \rightarrow C_2H_2 + 3H_2$ & $C_2H_2 \rightarrow 2C + H_2$), respectively. Each model is expressed as an equation that relates the kinetic constants to the residence time under the following assumptions:

- All reactions follow first-order kinetics.
- Both reactant and product gases behave as ideal gases.
- All gas species flow under steady-state conditions.

4.1. Selected kinetic models

Model 1 incorporates the effect of volume expansion due to gas-phase reactions [11]. The rate equation for this model is expressed as (3).

$$k\tau = -(1+\varepsilon)ln\,(1-X_{CH4}) - \varepsilon X_{CH4}, \qquad (3)$$

k is the kinetic rate constant, τ is the residence time, ε is the volume expansion factor, defined as the fractional change in molar volume due to reaction. This model assumes that the reaction behaves ideally, and that the volume change arises from stoichiometric difference between reactants and products.

Model 2 generalizes the previous two models by introducing two distinct factors: the chemical expansion factor α, and physical dilatation factor β [12]. The equation can be defined as (4).

$$k\tau = -\left(1+x_{CH4,0}\right)\beta\, ln(1-X_{CH4}) - x_{CH4,0}\beta X_{CH4}, \qquad (4)$$

This model separates chemical and physical influences on residence time and reaction, offering greater flexibility and accuracy for reaction calculation under non-ideal conditions. Residence time (τ) is determined from the total flow rate and reactor volume applying (5).

$$\tau = \frac{V_{reactor}}{Q_{total}}, \quad (5)$$

Where $V_{reactor}$ is the reactor volume [m^3] and Q_{total} is the total volumetric flow rate of gas inside reactor [m^3/s]. Using the kinetic expressions described in Model 1, 2 kinetic constants k can be determined by fitting the experimental methane conversion data. The temperature dependence of k follows the Arrhenius equation, as given by (6).

$$k = k_0 exp\left(\frac{-E_a}{RT}\right), \quad (6)$$

Where k_0 is pre-exponential factor [s^{-1}], E_a is activation energy [kJ/mol], R is gas constant [8.314 J/mol·K], and T is reactor temperature [K]. To estimate the kinetic parameters of k_0 and E_a, non-linear regression analysis was performed using MATLAB software. This fitting was independently applied to each of the three proposed kinetic models to evaluate the most appropriate expression that reflects the experimental results of methane pyrolysis under various operating conditions.

4.2. Model parameter tunning results

Table 4 summarizes the data fitting results of each model. Pre-exponential factors were measured ranging from $5.39 \cdot 10^4$-$4.94 \cdot 10^5$ s^{-1} and activation energy 141.01-155.46 kJ/mol and Figure 7 illustrates the three-dimensional profiles of methane conversion predicted by Model 1 and Model 2 across a temperature range of 700-1700 K and an initial concentration range of 0.1-0.9 at a constant residence time of 0.5. While both models are formulated based on a single global reaction ($CH_4 \rightarrow C + 2H_2$), they employ distinct mathematical frameworks to account for the volumetric expansion resulting from the increase in total moles during the pyrolysis process. Model 1 utilizes the standard expansion factor ε to represent volume change, whereas Model 2 incorporates a modified term involving the initial mole fraction $x_{CH4,0}$ and β coefficient to more rigorously capture the non-linear coupling between reactant concentration and gas-phase dilution within the plug flow reactor.

The simulation results reveal significant differences in the predicted reaction onset and temperature-dependent sensitivity between the two modeling approaches. Due to the lower optimized activation energy of Model 2 (141.01 kJ/mol) compared to Model 1 (155.46 kJ/mol), the initiation of methane decomposition, defined at 1% conversion, is predicted to occur at 1095.4 K in Model 2 at a 0.5 initial concentration. This is approximately 23.5 K lower than the 1118.9 K predicted by Model 1, suggesting that Model 2 exhibits higher sensitivity to the thermal activation of methane in the lower temperature regime. These findings indicate that the mathematical structure of Model 2 may more effectively represent the initial stages of decomposition where the reaction kinetics are primarily governed by the energy barrier under dilute conditions.

However, as the system moves into high-temperature and high-concentration regimes, Model 2 exhibits a pronounced non-linear suppression of conversion compared to the monotonic increase observed in Model 1. To achieve a target conversion of 90% at an initial concentration of 0.5, Model 2 requires an operating temperature of 1731.6 K, which represents a significant thermal requirement of nearly 80 K more than 652.2 K estimated by Model 1. This divergence highlights that the refined expansion terms in Model 2 impose a stricter kinetic penalty as the methane partial pressure increases, likely due to a more aggressive estimation of the residence time reduction caused by gas-phase expansion. Consequently, the comparative analysis suggests that while Model 1 provides a generalized global trend, Model 2 offers a more conservative and rigorous prediction for high-throughput reactor designs where near-complete conversion is required.

Table 4. *Data fitting results for single reaction.*

Parameter	Model 1	Model 2
k_0 [1/s]	$4.94 \cdot 10^5$	$5.39 \cdot 10^4$
E_a [kJ/mol]	155.46	141.01
R^2 [%]	87.71	89.78

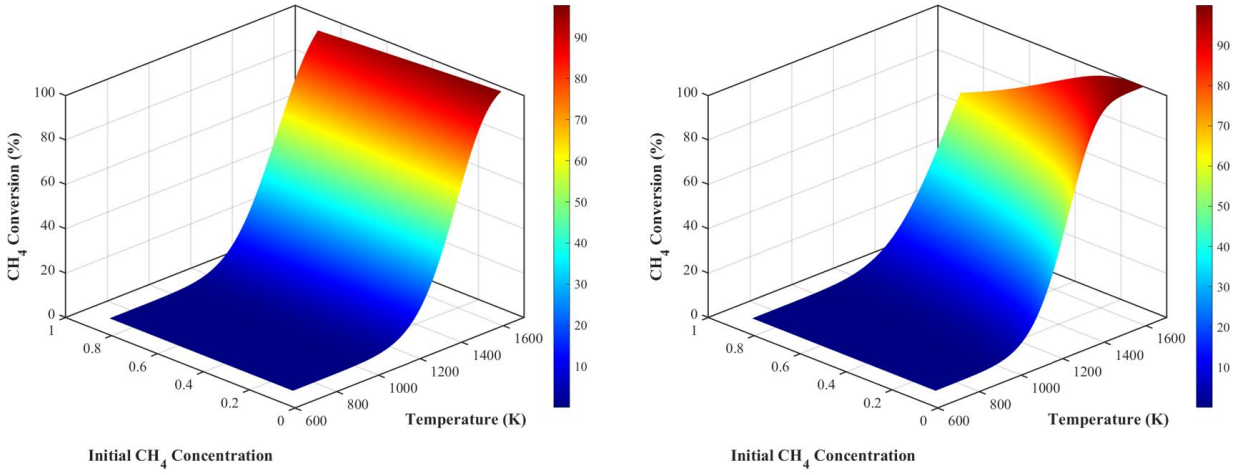

Figure. 7. *Comparison of predicted CH_4 conversion profiles between (a) Model 1 and (b) Model 2 as a function of reaction temperature (700-1700 K) and initial CH4 concentration (0.1-0.9) at a fixed residence time (τ=0.5 s)*

Table 5 presents the optimized kinetic parameters for the proposed 2-step series reaction mechanism, derived from the experimental data fitting. The primary step involves the decomposition of methane into acetylene and hydrogen ($2CH_4 \rightarrow C_2H_2 + 3H_2$). The subsequent step accounts for the decomposition of acetylene into solid carbon and hydrogen ($C_2H_2 \rightarrow 2C + H_2$), with an E_a of 94.14 kJ/mol. This lower activation energy for the second step relative to the first suggests that once formed, acetylene is readily susceptible to further decomposition into carbon at elevated temperatures.

To validate the reliability of the optimized kinetic parameters, the 2-step model was implemented into a PFR simulation to compare the predicted species profiles with the experimental results at 1300°C, as shown in Figure 8. Overall, the simulation (solid lines) successfully captures the experimental trends (dots) for CH_4, H_2, C_2H_2 across varying initial methane concentrations (1/4, 1/3, 1/2).

Specifically, the model accurately predicts the increase in H_2 mole fraction and the corresponding decrease in CH_4 with increasing initial concentration. For the intermediate species, C_2H_2, the model reasonably follows experimental behavior, although a slight deviation is observed at the 1/2 concentration ratio.

Table 5. *Optimized kinetic parameters for the two-step methane pyrolysis reaction*

Reaction	k_0 [1/s]	E_a [kJ/mol]	Description
$2CH_4 \rightarrow C_2H_2 + 3H_2$	$6.22 \cdot 10^5$	177.82	Methane decomposition & Acetylene formation
$C_2H_2 \rightarrow 2C + H_2$	$6.99 \cdot 10^3$	94.14	Acetylene decomposition & Carbon formation

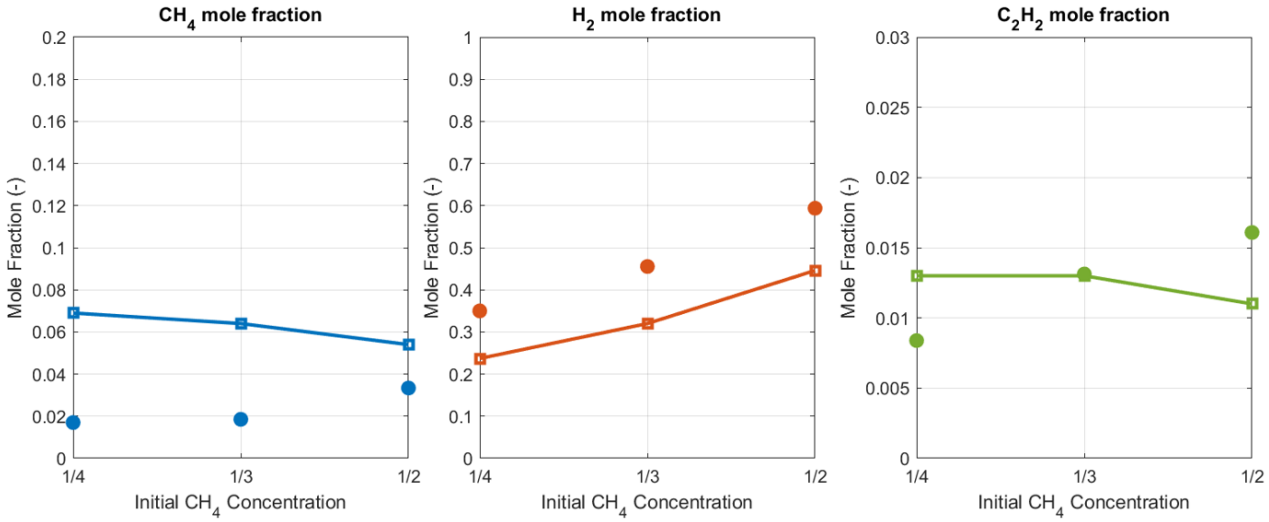

Figure. 8. *Comparison of experimental data and simulation results for the two-step reaction model at 1300 °C*

5. Conclusion

This study investigated the non-catalytic methane pyrolysis process through an integrated approach combining process simulation, high-temperature experiments, and kinetic modeling. The experimental results demonstrated that thermal energy is the dominant factor in overcoming kinetic barriers, achieving a maximum methane conversion of 97% at 1400 °C. Notably, decreasing the initial methane concentration significantly enhanced the hydrogen yield by suppressing the formation of secondary hydrocarbon byproducts. Conversely, at the lower temperature of 1200 °C, significant accumulation of intermediate acetylene was observed, indicating a kinetic bottleneck in the subsequent carbon formation step.

To accurately capture these complex behaviors, kinetic modeling was performed separating the mathematical expansion models and the reaction mechanisms. For the single-step global reaction, two distinct PFR mathematical equations were compared. The 3D parametric mapping revealed that Model 2, which incorporates a modified concentration-dependent expansion term, more rigorously predicts the non-linear kinetic penalties associated with high methane concentrations compared to the standard Model 1. Furthermore, to capture the intermediate species dynamics observed in the experiments, a two-step series reaction model was developed. The optimized two-step model validated the experimental concentration profiles of CH_4, H_2, C_2H_2, proving its reliability in predicting competitive reaction pathways.

As detailed in Appendix A, the operational stability assessment confirmed that scaling up the reactor inner diameter from 23 mm to 50 mm drastically mitigated preventing carbon clogging, enabling stable hydrogen production for over 12 hours. Ultimately, the derived kinetic parameters, combined with the 3D operational maps and scale-up strategies, present reliable and computationally efficient guidelines for the design and industrial deployment of carbon-free methane pyrolysis systems. In future work, the derived macroscopic kinetic models will be integrated into Computational Fluid Dynamics (CFD) simulations to conduct a comprehensive analysis of the reactor's thermochemical and fluid dynamics. Furthermore, more detailed experimental investigations will be performed to quantify other intermediate hydrocarbons—such as ethylene, ethane, and propane—in addition to acetylene. This expanded species mapping will further enhance the accuracy, precision, and robustness of the multi-step kinetic modeling framework for optimizing large-scale reactor designs.

Acknowledgments

This study was supported by the Korea Agency of Infrastructure Technology Advancement (KAIA) funded by the Korea government (MOLIT) (Grant number RS-2025-02303377).

Appendix A

Figure A1 presents the results of continuous operation tests conducted to evaluate the long-term stability of the methane pyrolysis process as a function of reactor ID. At a constant reaction temperature of 1300 °C, the 50 mm ID reactor demonstrated robust operational durability, maintaining 90% methane conversion for 12 hours of continuous stream time.

In contrast, the operation using the 23 mm ID reactor was significantly limited, with the test terminating prematurely within one hour. This abrupt termination is primarily due to the rapid accumulation of carbonaceous deposits (coking) within the reactor inside, which leads to an exponential increase in pressure drop and eventual reactor clogging. These results underscore that increasing the reactor ID from 23 mm to 50 mm effectively mitigates the clogging issues associated with solid carbon formation, thereby extending the continuous operation time and improving the overall reliability of the hydrogen production system.

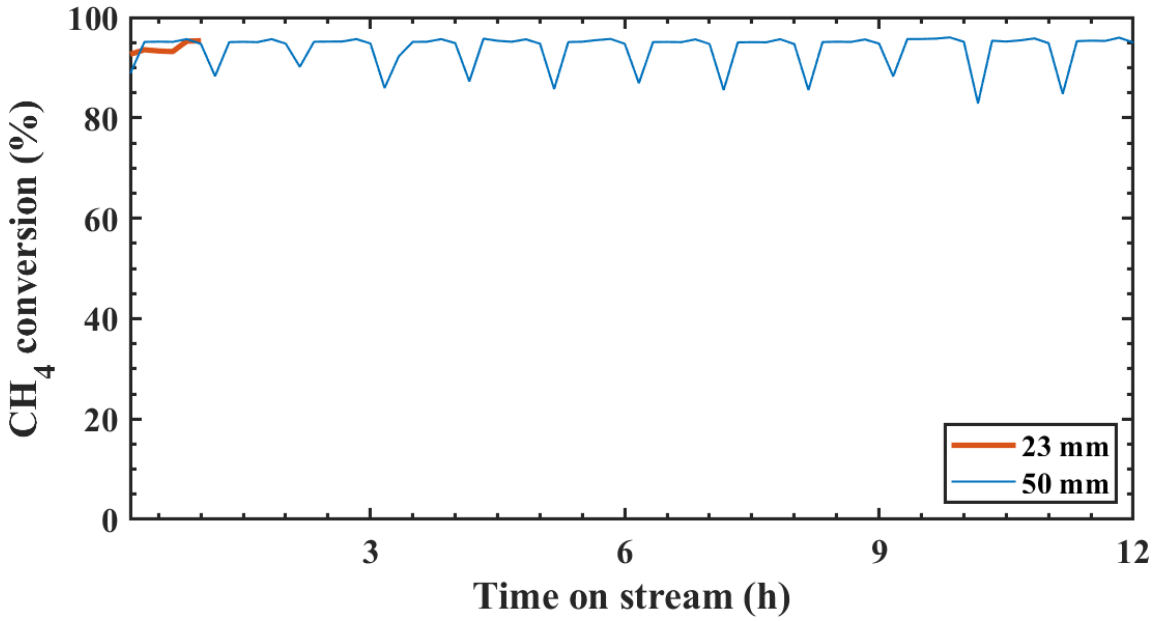

Figure. A.1. *Comparative analysis of long-term operational stability and CH_4 conversion trends for different reactor ID (23, 30 mm) at 1300 °C*

Nomenclature

E_a	activation energy	[kJ/mol]
k	kinetic constant	[1/s]
k_0	pre-exponential factor	[1/s]
$Q_{CH4,in}$	Inlet flow rate of CH_4	[Lpm]
$Q_{CH4,out}$	Outlet flow rate of CH_4	[Lpm]
$Q_{CH4,reaction}$	Flow rate of reactions CH_4	[Lpm]
R	gas constant	[$JK^{-1}mol^{-1}$]
$x_{CH4,0}$	initial CH_4 mole fraction	[–]
X_{CH4}	CH_4 conversion	[%]

Greek symbols

β physical dilatation factor

ε volume expansion factor

τ residence time

References

[1] Ji M, Wang J. Review and comparison of various hydrogen production methods based on costs and life cycle impact assessment indicators. Int J Hydrogen Energy 2021;46:38612–35. https://doi.org/10.1016/j.ijhydene.2021.09.142.

[2] Holmerp A, Olsvikb O, Rokstad OA. Pyrolysis of natural gas: chemistry and process concepts. vol. 42. ELSEVIER; 1995.

[3] Upham DC, Agarwal V, Khechfe A, Snodgrass ZR, Gordon MJ, Metiu H, Mcfarland EW. Catalytic molten metals for the direct conversion of methane to hydrogen and separable carbon. 1000.

[4] Lott P, Mokashi MB, Müller H, Heitlinger DJ, Lichtenberg S, Shirsath AB, Janzer C, Tischer S, Maier L, Deutschmann O. Hydrogen Production and Carbon Capture by Gas-Phase Methane Pyrolysis: A Feasibility Study. ChemSusChem 2023;16:e202201720. https://doi.org/10.1002/cssc.202201720.

[5] Dahl JK, Barocas VH, Clough DE, Weimer AW. Intrinsic kinetics for rapid decomposition of methane in an aerosol low reactor. vol. 27. 2002.

[6] Trommer D, Hirsch D, Steinfeld A. Kinetic investigation of the thermal decomposition of CH4 by direct irradiation of a vortex-flow laden with carbon particles. Int J Hydrogen Energy 2004;29:627–33. https://doi.org/10.1016/j.ijhydene.2003.07.001.

[7] Rodat S, Abanades S, Coulié J, Flamant G. Kinetic modelling of methane decomposition in a tubular solar reactor. Chemical Engineering Journal 2009;146:120–7. https://doi.org/10.1016/j.cej.2008.09.008.

[8] Çelik A, Shirsath AB, Syla F, Müller H, Lott P, Deutschmann O. On the role of hydrogen inhibition in gas-phase methane pyrolysis for carbon capture and hydrogen production in a tubular flow reactor. J Anal Appl Pyrolysis 2024;181. https://doi.org/10.1016/j.jaap.2024.106628.

[9] Koshi M, Uehara T, Asahara M. Problems in the reaction mechanism of methane pyrolysis for hydrogen production. Int J Hydrogen Energy 2024;72:850–60. https://doi.org/10.1016/j.ijhydene.2024.05.305.

[10] Vargas J, van Rooij GJ, Diomede P. Methane plasma pyrolysis chemical kinetics: Dominant pathways and model reduction. Next Chemical Engineering 2026;2:100020. https://doi.org/10.1016/j.nxcen.2026.100020.

[11] Levenspiel O. Chemical reaction engineering. 3rd ed. New York: Wiley; 1999.

[12] Abanades S, Flamant G. Hydrogen production from solar thermal dissociation of methane in a high-temperature fluid-wall chemical reactor. Chemical Engineering and Processing: Process Intensification 2008;47:490–8. https://doi.org/1